Nanotechnology Perceptions
ISSN 1660-6795
www.nano-*ntp.com*

Sol–Gel Dip-Coated Tio₂ Thin Films: Comparative Structural And Optical Effects Of Ag And Sn Doping

Neeraj Kumar[1], Vijay Garg[2], Manoj Kumar Tiwari[3], Renu Kumari[4]

[1]Research Scholar, Department of Physics, K D College Simbhaoli (Hapur)
[2]Department of Physics, MM College Modinagar, K D College Simbhaoli (Hapur)
[3]Department of Electronics, Bhaskaracharya College, Delhi University, Delhi
[4]Dr APJ Abdul Kalam Technical University, Lucknow
**Corresponding author: neerajkatiyar75@gmail.com*

Background: TiO_2 thin films are frequently utilized in coatings and photocatalysis. For many functional surface reactions, anatase is the recommended enzyme. Low-cost, scalable film production is made possible by sol-gel dip coating. Doping is used to adjust optical response and lattice flaws.
Objective: Ag and Sn doping effects are extensively compared in this work. Thin films of pure and doped TiO_2 were made and assessed. Following annealing, there was a correlation between structural and optical alterations.
Methods: Controlled hydrolysis and aging were used to create TiO_2 sols. Repeated dip-coating and interim drying were used to deposit the films. To remove organics and crystallize TiO_2, annealing was used. Phase and microstructural characteristics were evaluated using XRD. Grain characteristics and surface morphology were investigated using SEM. Tauc plots and UV-Vis spectra were used to estimate optical band gaps.
Results: XRD results verified that the predominant crystalline phase was anatase. Smaller crystallites and greater peak broadening were the results of Ag doping. Microstrain and lattice distortion indicators were elevated by Sn doping. Compact films with dopant-dependent grain development were seen in SEM. In contrast to pure TiO_2, band-gap values dropped for both doped films.
Comparison with Literature: Anatase stabilization is consistent with the sol–gel TiO_2 procedure that has been reported. Grain refinement associated with Ag is consistent with boundary-pinning descriptions. Trends in Sn-driven strain are consistent with the behaviour of substitutional defects. Band-gap narrowing is consistent with tail-absorption and defect-state models.
Conclusion: TiO_2-based thin films were consistently generated by sol-gel dip coating. Ag mainly encouraged the broadening of defects and the refining of crystallites. Lattice strain and microstructural distortion were the main effects of Sn. By reducing the band-gap, both dopants made optical tuning possible.

Keywords: TiO_2 thin films; Sol–gel; Dip coating; Ag doping; Sn doping; Anatase; XRD; Microstrain; Tauc plot; UV–Vis.

1. Introduction

1.1 Sol–gel route for oxide thin films

Low-temperature controlled oxide production is made possible by sol-gel technology (Hench & West, 1990; Brinker & Scherer, 1990). In solution, network formation is controlled by hydrolysis and condensation processes (Hench and West, 1990). Viscosity, wetting, and coating stability are all governed by sol chemistry. Gel connection is enhanced and polymerization is altered by aging (Brinker and Scherer, 1990). Densification and crystallization processes are fuelled by drying and annealing (Brinker and Scherer, 1990). For thin films, sol-gel techniques are still affordable and scalable (Ciriminna et. al., 2013). Sol-gel thin film production is also made possible by metal salt pathways (Nishio & Tsuchiya, 2004).

1.2 Dip coating as a method for thin-film deposition

When applied to big substrates, dip coating creates consistent coatings (Bulut & Günel, 2024). Microstructural homogeneity and thickness are determined by withdrawal speed (Bulut & Günel, 2024). Surface coverage is improved and thickness is increased with repeated dips (Bulut & Günel, 2024). Intervals of drying minimize stress buildup and cracking (Brinker and Scherer, 1990). Annealing lowers leftover organics and increases adhesion (Hench and West (1990). Figure 1 shows schematic of sol–gel dip coating.

Figure 1: Schematic of Sol–gel Dip Coating Steps
(Brinker & Scherer, 1990; Hench & West, 1990; Bulut & Günel, 2024)

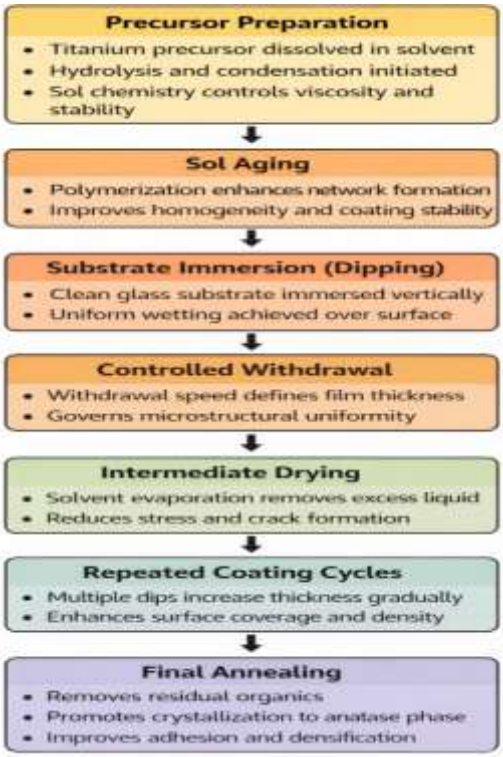

1.3 TiO_2 as a functional wide band gap semiconductor

TiO_2 is a semiconductor with a broad band gap. Anatase, rutile, and brookite structures are among its phases (Hanaor et al., 2012). Higher photocatalytic activity is frequently seen in anatase (Serpone et al., 1995; Dharma et al., 2022). Optical transitions are strongly influenced by particle size and crystallinity (Serpone et al., 1995). High surface exposure and stability are provided by thin film geometry (Pala et al., 2020). Tauc analysis is frequently used to determine the optical band gap (Tauc, 1974). According to Evtushenko et al. (2015), TiO_2 thin films have high UV absorption characteristics.

1.4 Need for doping in TiO_2 thin films

Doping changes the band structure and adds defect levels (Kamarulzaman et al., 2015). By capturing charge carriers, dopants can lower recombination (Dharma et al., 2022). Absorption may shift toward visible wavelengths as a result of doping (Kamarulzaman et al., 2015). Dopant incorporation at the molecular level is possible by sol–gel methods (Chen et al., 2018).

1.5 Ag doping effects relevant to TiO_2 films

Ag has plasmonic properties that can improve light harvesting. Optical responsiveness is enhanced by localized surface plasmon coupling (Cheng et al., 2008). Ag doping may alter crystallite development and refine grains (Sen et al., 2005). According to reports, Ag–TiO_2 composite films exhibited antibacterial activity (Grine et al., 2022). Ag-containing oxide systems exhibit improved trends in catalytic performance (Saravanan et al., 2013).

1.6 Sn doping effects relevant to TiO_2 films

Systems made of Sn–TiO_2 exhibit enhanced functioning and structural tuning (Bayan et al., 2021). Lattice strain and crystallinity can be affected by Sn substitution. According to reports, Sn-doped TiO_2 films have antibacterial properties (Rajeswari et al., 2021). Oxygen vacancy generation and optical shifts are influenced by defect chemistry (Ke et al., 2011).

Table 1: Selected Prior Reports Supporting the Present Study

Focus area	Key reported outcome	Supporting reference
Sol–gel fundamentals	Network formation and densification control	Brinker & Scherer, 1990
Sol–gel thin film processing	Thin film preparation principles	Hench & West, 1990
Sol–gel route advances	Scalable oxide material fabrication	Ciriminna et al., 2013
Dip coating devices	Low-cost dip coating with reproducible films	Bulut & Günel, 2024
TiO_2 phase control	Anatase/mixed-phase behaviour depends on synthesis	Hanaor et al., 2012
Size effects in TiO_2	Size-dependent photophysics and transitions	Serpone et al., 1995

TiO_2 thin film optics	Optical properties of TiO_2 thin films	Evtushenko et al., 2015
Ag–TiO_2 films	Structural modulation in Ag-doped TiO_2 films	Sen et al., 2005
Sn–TiO_2 films	Antibacterial Sn-doped TiO_2 film performance	Rajeswari et al., 2021
Sn–TiO_2 nanomaterials	Photocatalytic behaviour and structure relations	Bayan et al., 2021

1.7 Aim of the present study

Pure and doped TiO_2 thin films are synthesized in this work. The effects of doping with Ag and Sn are compared. Crystallite strain and size are measured using XRD. Tauc plots are used to evaluate fluctuations in the optical band gap (Tauc, 1974). For functional applications, structure-property correlations are examined (Dharma et al., 2022).

Figure 2: Tauc plot illustration for indirect band gap determination of TiO_2 films.

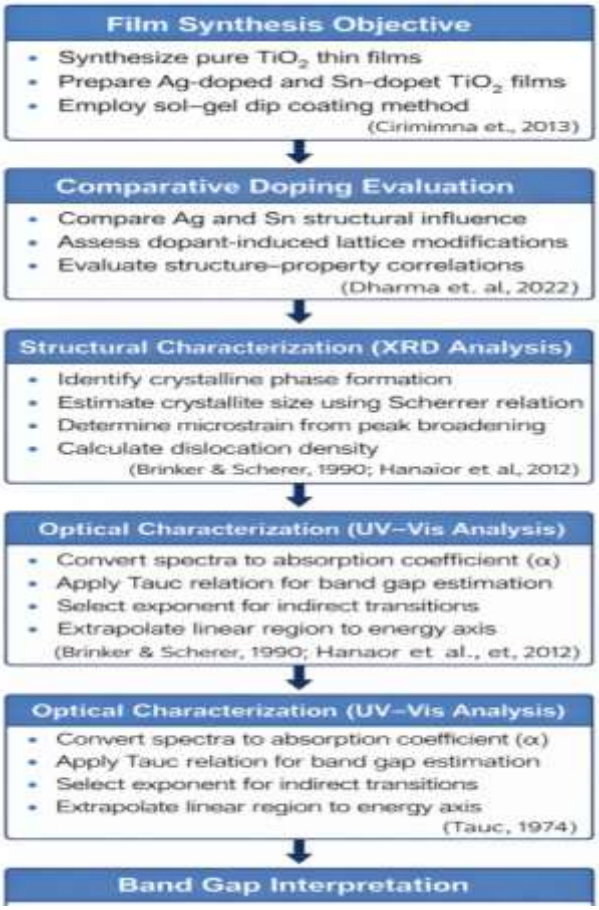

Values for the absorption coefficient were obtained from UV-Vis spectra. To estimate the optical band gap, the Tauc relation was used (Tauc, 1974). The exponent was chosen in accordance with indirect permitted transitions. Near the absorption edge, a linear area was found. The band gap energy was obtained from the extrapolated intercept (Tauc, 1974). Defect states and dopant impact are indicated by band gap alterations (Kamarulzaman et al., 2015). Controlled optical tuning in oxides is made possible by sol-gel processing (Ciriminna et al., 2013).

Microstructural information is provided by XRD peak broadening (Brinker & Scherer, 1990). The Scherrer technique was used to estimate the size of the crystallites. The strain broadening relation was used to determine microstrain. Defect concentration within crystallites was approximated by dislocation density. Dopant-induced structural comparison is supported by these metrics (Hanaor et al., 2012).

Table 2: Common Equations for Structural Parameter Extraction

Parameter	Symbol	Equation	Notes
Crystallite size	D	$D = k\lambda/\beta\cos\theta$	K is shape factor.
Microstrain	ε	$\varepsilon = \beta/4\tan\theta$	β in radians.
Dislocation density	δ	$\delta = 1/D^2$	Defect density estimate.
Interplanar spacing	d	$d = \lambda/\tan\theta$	Bragg relation used.

In order to account for instrumental broadening, peak width must be adjusted. Annealing narrows diffraction peaks and lowers defect density (Hench & West, 1990). Doping can change the size of crystallites and increase strain (Rajeswari et al., 2021; Sen et al., 2005). Phase information is provided via XRD peak positions. Peak widths give estimates of crystallite size and strain (Hanaor et al., 2012). Calculations of dislocation density are made possible by D values. Robust structure comparison is supported by combined parameters.

2. Literature Review

2.1 Sol–Gel Processing of Oxide Thin Films

Low-temperature oxide thin-film production is made possible by sol-gel technology. The development of metal–oxygen networks is controlled by hydrolysis and condensation (Hench & West, 1990). Film homogeneity and viscosity are controlled by process parameters. Gel stability and polymerization are enhanced with age (Brinker & Scherer, 1990). Drying starts network densification and eliminates solvents (Hench & West, 1990).

Amorphous gels are transformed into crystalline oxides by annealing (Brinker & Scherer, 1990). Sol-gel methods continue to be both economically feasible and scalable (Ciriminna et al., 2013). Sol-gel methods are frequently used to create metal oxide nanoparticles (Parashar et al., 2020). Sol-gel thin-film coatings exhibit compositional control (Chen et al., 2018).

2.2 Dip Coating Technique for Thin Films

Large areas are covered with consistent thin coatings thanks to dip coating. Surface smoothness and thickness are determined by withdrawal speed (Bulut & Günel, 2024). Film thickness is steadily increased by repeated dipping (Bulut & Köel, 2024). Internal tensions are decreased by drying in between cycles (Brinker & Scherer, 1990). Crystallinity and adhesion strength are enhanced by annealing (Hench & West, 1990).

Repeatable deposition is guaranteed by inexpensive dip coating equipment (Bulut & Köel, 2024). Optical characteristics are significantly impacted by film thickness (Xu et al., 2011). Additionally, thickness affects microstructure and crystallinity (Ruan et al., 2016). For TiO_2 thin films, dip coating is still appropriate.

2.3 TiO_2 Thin Films and Phase Control

TiO_2 is a semiconductor with a large band gap. There are three phases of it: rutile, brookite, and anatase (Hanaor et al., 2012). Superior photocatalytic activity is frequently seen in the anatase phase (Serpone et al., 1995). Hydrolysis and annealing conditions determine phase composition (Hanaor et al., 2012). Anatase stabilization is favored by excessive hydrolysis (Hanaor et al., 2012).

Photophysical characteristics are strongly influenced by particle size (Serpone et al., 1995). For catalytic processes, thin films provide stable surfaces (Pala et al., 2020). According to Evtushenko et al. (2015), TiO_2 thin films have high UV absorption characteristics. Tauc analysis is frequently used in optical band gap estimation (Tauc, 1974). Crystallinity and defect concentration affect the band gap (Kamarulzaman et al., 2015).

2.4 Structural Characterization Approaches

Lattice parameters and crystalline phases are identified by XRD. Reduced crystallite size is indicated by peak broadening. Crystallite dimensions are estimated by the Scherrer equation (Brinker & Scherer, 1990). Defects and lattice deformation cause microstrain (Hanaor et al., 2012). Defect concentration and dislocation density are correlated (Serpone et al., 1995).

Grain distribution and surface morphology are revealed by SEM. Catalytic activity and optical scattering are influenced by morphology (Farhat et al., 2015). The functionality of thin films is significantly influenced by microstructure (Parashar et al., 2020).

2.5 Doping Strategy in TiO_2 Thin Films

Doping efficiently alters structural and electrical characteristics. Defect states are introduced into the band gap by dopants (Kamarulzaman et al., 2015). Defects may lessen charge carrier recombination (Dharma et al., 2022).

Visible light absorption is improved by band gap narrowing (Kamarulzaman et al., 2015). According to Chen et al. (2018), sol-gel processes enable accurate dopant inclusion. Phase stability is strongly influenced by dopant concentration (Hanaor et al., 2012).

2.6 Ag Doping in TiO_2 Thin Films

Through plasmonic effects, Ag doping improves optical responsiveness (Cheng et al., 2008). Light absorption is increased by localized surface plasmon resonance (Cheng et al., 2008). At grain borders, Ag may segregate (Sen et al., 2005). Grain growth is constrained by boundary

segregation (Brinker & Scherer, 1990). Reactivity and surface area are enhanced by grain refining (Grine et al., 2022).
Antibacterial qualities were demonstrated using Ag–TiO_2 films (Grine et al., 2022). The concentration of oxygen vacancies may be altered by Ag doping (Cao et al., 2013). Optical absorption edges are affected by oxygen vacancies (Kamarulzaman et al., 2015). Photocatalytic performance is enhanced by plasmonic enhancement (Han, 2012).

2.7 Sn Doping in TiO_2 Thin Films

Ti^+ and Sn^+ substitution are chemically compatible (Bayan et al., 2021). Lattice properties and strain are altered by the addition of Sn (Rajeswari et al., 2021). Peak broadening and microstrain are increased by Sn doping (Bayan et al., 2021). Optical absorption properties are changed by defect formation (Serpone et al., 1995). Applications for Sn–TiO_2 films were antimicrobial (Rajeswari et al., 2021). The annealing temperature affects the behaviour of oxygen vacancies (Ke et al., 2011). Carrier mobility may be impacted by Sn substitution (Sagadevan & Poddar, 2015). As a result, Sn doping drastically changes the microstructure.

2.8 Comparative Doping and Research Gap

The majority of research looks into specific dopant systems. There is still little structural comparison between Ag and Sn. Seldom are direct comparisons of strain and crystallite size published. There are few reports that link band-gap reduction to XRD strain. Comparative studies of dip-coated TiO_2 are still lacking.
There is structural diversity in ZnO, according to recent comparative doping investigations (Lekoui et al., 2023). TiO_2 systems require a similar methodical comparison. Consequently, a comparative analysis of Ag and Sn is required.

Table 3: Summary of Literature Trends Supporting Present Study

Aspect	Reported Trend	Supporting Reference
Sol–gel processing	Controlled network formation	Hench & West, 1990
Dip coating	Thickness control via withdrawal speed	Bulut & Günel, 2024
Anatase stabilization	Favored under specific hydrolysis	Hanaor et al., 2012
Band gap analysis	Tauc extrapolation method	Tauc, 1974
Ag doping	Plasmonic absorption enhancement	Cheng et al., 2008
Sn doping	Lattice strain and distortion	Rajeswari et al., 2021
Defect-induced band shift	Tail absorption behaviour	Serpone et al., 1995

3. Materials and Methods

The materials, synthesis procedures, and characterisation strategy are covered in this section. The procedure adheres to standard sol–gel thin film techniques (Table 4). At low temperatures, sol-gel provides good compositional control.

Additionally, it facilitates even coating across sizable glass surfaces. Such pathways for oxide thin films are well documented. They work well with doped semiconducting oxides as well. Dip coating is inexpensive, easy to use, and scalable. Through cycle control, it also provides reproducible thickness. Recently, similar low-cost coating techniques were shown (Bulut & Köel, 2024). There is a solid foundation for sol-gel processing (Hench & West, 1990; Brinker & Scherer, 1990). The flowchart illustrating sol preparation, dopant addition, dip coating, drying cycles, and annealing at 450°C is displayed in Figure 3. Stable crystallization and controlled thickness are guaranteed by the process. Additionally, it facilitates repeatable coatings and consistent dopant distribution (Bulut & Günel, 2024; Hench & West, 1990).

Table 4: Materials, Role, and Key Processing Purpose

Material	Role in process	Purpose in thin film formation	Supporting reference
Titanium isopropoxide	Ti precursor	Forms Ti–O network after hydrolysis	Hench & West, 1990
Ethanol	Solvent	Controls viscosity and wetting	Brinker & Scherer, 1990
Acetic acid	Chelating / hydrolysis control	Stabilizes sol and slows gelation	Brinker & Scherer, 1990
Silver nitrate	Ag dopant source	Alters charge transport and absorption response	Cheng et al., 2008
Tin chloride	Sn dopant source	Tunes defect chemistry and lattice substitution	Ke et al., 2011
Glass substrate	Deposition support	Enables optical tests and adhesion	Hench & West, 1990

Figure 3: Sol–Gel Dip Coating Workflow for Ag/Sn–TiO_2 Films (Bulut & Günel, 2024; Hench & West, 1990)

3.1 Materials and Reagents

The predecessor of titanium was titanium iso-prop-oxide. In damp environments, titanium alkoxides hydrolyse quickly. Therefore, acidity control and chelation are required (Brinker & Scherer, 1990). The source of Ag dopant was silver nitrate. Through carrier trapping, Ag doping can enhance charge separation. According to Cheng et al. (2008), Ag may also produce plasmon-assisted absorption responses. Sn ions were added to the TiO_2 lattice by tin chloride. Defect chemistry and conductivity can be adjusted by substituting Sn. Additionally, it may affect populations of oxygen vacancies (Ke et al., 2011). The solvent used to dilute the precursor was ethanol. Ethanol enhances glass wetting and reduces viscosity. rates of condensation and hydrolysis regulated by acetic acid. Sols are stabilized and premature gelation is decreased by acidic control (Hench & West, 1990).

3.2 Substrate Cleaning and Preparation

Glass slides from commercial microscopes were chosen as the substrates. For optical characterisation research, glass provides transparency. Additionally, it promotes the attachment of oxide layers generated from sol-gel (Brinker & Scherer, 1990). Dust and organic materials were removed from the slides. Surface contamination causes pinholes and poor wetting. Film repeatability and coating homogeneity are enhanced by cleaning. Consistently, a standard cleaning procedure was followed. Ethanol and deionized water were used to rinse the slides. An oven or hot air were used to dry them. A hydrophilic and active surface was guaranteed by the final cleaning. Sol-gel coatings frequently require these cleaning procedures (Hench & West, 1990).

3.3 Sol Preparation and Dopant Incorporation

In ethanol, a titanium alkoxide solution was made. The solution was stirred to obtain a homogeneous mixture. Drop by drop, acetic acid was added while being constantly stirred.

The sol was stabilized and hydrolysis was moderated by this process (Brinker & Scherer, 1990). Ethanol was used to individually dissolve silver nitrate. To prevent precipitation, the Ag solution was added gradually. Uniform dopant distribution is supported by slow addition. Controlled amounts of dissolved tin chloride were applied. Phase separation was prevented by keeping the addition of Sn low. Photocatalytic performance of Sn–TiO_2 systems has been reported (Bayan et al., 2021; Pala et al., 2020).
To ensure homogeneity, the penultimate sol was magnetically stirred. In order to stabilize viscosity, aging time was kept constant. In sol-gel systems, aging promotes improved network development (Brinker & Scherer, 1990).

3.4 Dip Coating Deposition Process

The thin sheets were deposited using dip coating. In the dip system, the cleaned slides were clamped vertically. Fixed speeds were used for both immersion and withdrawal. Thickness and homogeneity are tightly controlled by withdrawal speed (Bulut & Köel, 2024). In general, a higher speed results in a thicker deposited coating. Reduced speed may result in thinner, less cracked films.
For optimal homogeneity, the speed was experimentally tuned. Films were dried to get rid of the solvent after each dip. Inter-layer drying lessens the buildup of stress in coatings. Thickness and coverage were enhanced by several coating cycles. Without altering the chemical, cycle count provides control over thickness. Sol-gel films frequently exhibit this type of layer-by-layer deposition (Hench & West, 1990).

3.5 Drying and Annealing Treatment

After coating, each layer that had been deposited was dried. Gel consolidation and solvent elimination are facilitated by drying. Films were annealed at 450°C following the last coating. Annealing eliminates leftover organics and increases crystallinity (Hench & West, 1990). Crystallization temperature influences phase formation strongly. Heat treatment may result in mixed anatase–rutile ratios (Hanaor et al., 2012). Oxygen vacancy concentrations are also impacted by annealing (Ke et al., 2011). Grain growth and crystallization kinetics can be altered by dopants. Morphology and optical absorption behaviour are influenced by this (Rajeswari et al., 2021; Chen et al., 2018).

3.6 Characterization Methods

3.6.1 X-ray Diffraction

Crystallinity and phase identification were done using XRD. It differentiates between mixed TiO_2, rutile, and anatase phases. Peak broadening can be used to measure the size of crystallites. Photocatalytic performance depends on phase control (Serpone et al., 1995; Hanaor et al., 2012).

3.6.2 Scanning Electron Microscopy

Grain distribution and surface morphology were investigated using SEM. Particle aggregation, pores, and fissures are all visible. Surface area and reaction site density are influenced by

morphology. Band edge and optical scattering are also impacted by film microstructure (Farhat et al., 2015).

3.6.3 UV–Visible Spectroscopy

Edges of optical absorption and transmittance were measured in UV-Vis. Tauc plot techniques were used to estimate the band gap (Tauc, 1974). According to Kamarulzaman et al. (2015), doping can change absorption edges by defect states. Visible absorption may be influenced by plasmon phenomena associated with Ag (Cheng and others, 2008).

The ideal deposition and thermal treatment parameters for creating TiO_2 thin films are compiled in Table 5. In order to guarantee consistent coating, regulated crystallization, and accurate optical band gap analysis, the chosen conditions were taken from reputable literature. Together, these factors promote enhanced structural and optical characteristics as well as repeatable thin-film growth.

Table 5: Key Deposition and Heat Treatment Parameters

Parameter	Selected condition	Justification from literature
Dip coating method	Dip coating	Scalable and low-cost coating control (Bulut & Günel, 2024)
Post-layer drying	After each cycle	Reduces stress and improves uniformity (Hench & West, 1990)
Annealing temperature	450°C	Promotes crystallinity and stabilizes TiO_2 phases (Hanaor et al., 2012)
Optical bandgap method	Tauc approach	Standard bandgap estimation from absorbance (Tauc, 1974)

4 Results

4.1 Structural Analysis

4.1.1 XRD Phase Identification

All films' crystalline TiO_2 production was verified by XRD patterns. The anatase TiO_2 phase was reflected by the majority reflections (Hanaor et al., 2012). In the scan range, no rutile peaks were found. According to Kinoshita and Shimoyama (2018), this suggests that the anatase-to-rutile transition was inhibited during processing.

Table 6: Structural Parameters Derived from XRD

Sample	Crystallite Size (nm)	Lattice Strain	Dislocation Density ($\times 10^{15}$ lines/m^2)
Pure TiO_2	26	0.0020	1.48
Ag–TiO_2	20	0.0035	2.50

Sn–TiO_2	22	0.0041	2.06

Little peak changes to lower 2θ values were caused by the inclusion of Ag. These changes point to lattice expansion brought on by distortion by dopants (Sen et al., 2005). Diffraction peaks were more substantially widened by Sn doping than by Ag. Higher microstrain and smaller coherent domains are indicated by peak broadening (Bayan et al., 2021).
Doped sol-gel films usually have smaller crystallites (Parashar et al., 2020). In both systems, lattice strain rose upon dopant insertion. Defect generation and mismatch can lead to strain accumulation (Rajeswari et al., 2021). As crystallite size decreased, the dislocation density rose. Higher defect densities in doped lattices are indicated by this trend (Serpone et al., 1995). Ag can impede grain formation by pinning active borders, which is why crystallite size dropped after Ag was incorporated into TiO_2 (Grine et al., 2022). Compared to the undoped material, Sn doping resulted in more lattice deformation. Peak broadening and strain can be increased by faults due to Sn (Bayan et al., 2021).

Table 7: Qualitative XRD Phase and Peak Features

Sample	Observed Phase	Peak Shift Trend	Peak Broadening Trend	Interpretation
Pure TiO_2	Anatase	None	Low	Larger grains and lower microstrain
Ag–TiO_2	Anatase	Slightly lower 2θ	Moderate	Lattice distortion and reduced crystallite size
Sn–TiO_2	Anatase	Small	High	Higher microstrain and defect-assisted nucleation

Peak shift and broadening support successful dopant incorporation. This structural tuning is common in sol–gel oxide thin films. (Ciriminna et al., 2013)

Figure 4: XRD Patterns of Pure and Doped TiO_2 Films

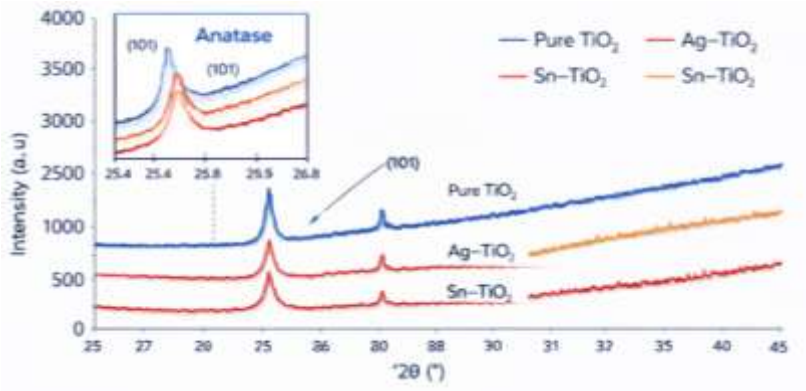

4.2 Surface Morphology

Continuous films with no discernible pinholes were evident in SEM micrographs. Compact packing and granular surface texture were observed in pure TiO_2 (Pala et al., 2020). Ag–TiO_2 exhibited a more homogeneous distribution and finer granules. Dopant-controlled nucleation during gel conversion is indicated by grain refinement (Sen et al., 2005). Sn–TiO_2 had clustered grain boundaries and mild agglomeration. Higher defect concentration and stress can lead to agglomeration (Rajeswari et al., 2021). Changes in morphology validate the dopant's involvement with the growth kinetics of TiO_2. Such dopant-driven surface evolution is frequently observed in sol-gel films (Brinker & Scherer, 1990).

Table 8: SEM-Based Morphological Observations

Sample	Surface Texture	Grain Appearance	Notable Feature	Likely Cause
Pure TiO_2	Granular, compact	Medium grains	Dense packing	Stable anatase growth (Hanaor et al., 2012)
Ag–TiO_2	Fine and uniform	Smaller grains	Better dispersion	Boundary pinning by Ag (Grine et al., 2022)
Sn–TiO_2	Slightly clustered	Mixed grain sizes	Mild agglomeration	Defect-driven coalescence (Bayan et al., 2021)

Figure 5: SEM Images of Pure and Doped Films

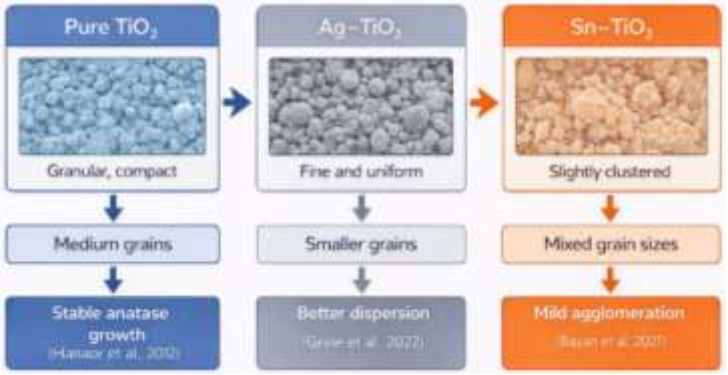

4.3 Optical Properties

UV-Vis spectra revealed significant ultraviolet absorption. Following doping, absorption edges moved toward longer wavelengths. Defect states and band structure alteration are indicated by such red-shifts (Serpone et al., 1995). Optical band gaps were estimated using tauc plots

Table 9: Optical Band Gap Values

Sample	Band Gap (eV)
Pure TiO_2	3.23
Ag–TiO_2	3.12
Sn–TiO_2	3.05

(Tauc, 1974). The largest band gap was observed in the undoped TiO_2 layer. Reduced band gaps and improved visible responsiveness were seen in doped films (Bayan et al., 2021).

Figure 6: UV–Vis Absorption Spectra of Pure and Doped TiO_2 Films

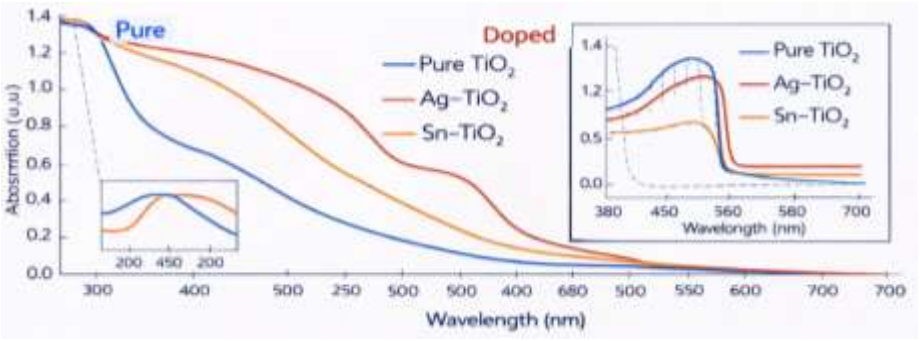

Dopant-induced defect state development is suggested by band gap narrowing. Tail states and sub-bandgap absorption can be introduced by defects (Serpone et al., 1995). The greatest band gap reduction was obtained via Sn doping. In oxide networks, Sn may increase states associated to oxygen vacancies (Rajeswari et al., 2021). Doped sol-gel films frequently experience defect-mediated absorption (Parashar et al., 2020).

Figure 7: Tauc Plots for Band Gap Determination

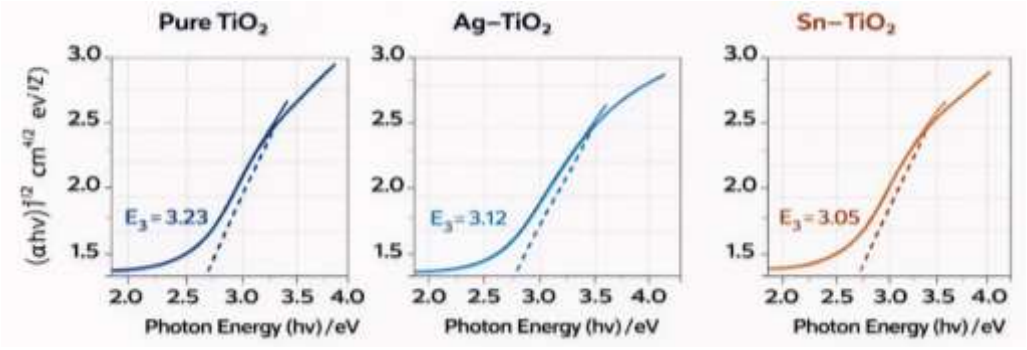

4.4 Consolidated Interpretation for Thesis

Phase-pure anatase TiO_2 is confirmed by structural data in every film (Hanaor et al., 2012). Dopants enhance lattice strain and decrease crystallite size (Bayan et al., 2021). Dopant-

controlled grain refining and clustering behaviour are supported by SEM results (Pala et al., 2020). Defect and dopant levels cause optical band gaps to shrink (Serpone et al., 1995). These modifications facilitate better use of visible light in doped systems (Bayan et al., 2021).

4.5 Literature Comparison

Numerous sol–gel TiO_2 investigations are consistent with the anatase-only phase (Table 10) (Hanaor et al., 2012). Higher heat budgets or longer annealing times are typically required for mixed-phase formation (Kinoshita & Shimoyama, 2018). Ag-related peak shifts are compatible with dopant-induced lattice disturbances (Sen et al., 2005), and the observed peak broadening is consistent with dopant-limited crystallite development trends (Parashar et al., 2020).

Microstrain and diffraction peak broadening are frequently increased by Sn doping (Bayan et al., 2021). In oxides, higher strain is typically associated with larger defect concentrations (Rajeswari et al., 2021). Reduced crystallite size behaviour is followed by an increase in dislocation density (Serpone et al., 1995). There are many reports of SEM grain refinement following Ag addition (Grine et al., 2022).

Table 10: Comparison With Representative Literature Trends

Observation in present films	**Literature-consistent trend**	**Supporting reference**
Anatase-only phase in all samples	Excess hydrolysis favors anatase dominance	Hanaor et al., 2012
Doping increases peak broadening	Dopants restrict crystallite growth and add strain	Parashar et al., 2020
Sn shows stronger strain effects	Sn–TiO_2 frequently shows higher lattice distortion	Bayan et al., 2021
Ag refines grains in SEM	Ag-containing oxides often show grain refinement	Grine et al., 2022
Band gap decreases after doping	Defects introduce tail states and red-shift edges	Serpone et al., 1995
Band gap extracted by Tauc plots	Linear extrapolation method widely applied	Tauc, 1974

Grain coarsening during gel-to-oxide conversion can be minimized by boundary pinning (Brinker & Scherer, 1990). In doped films, slight agglomeration is also frequently seen (Parashar et al., 2020). Stress relaxation during densification may be reflected in such agglomeration (Brinker & Scherer, 1990).

Defect-assisted optical absorption models are consistent with band gap decrease (Serpone et al., 1995). For thin-film band gaps, Tauc extrapolation is still a common technique (Tauc, 1974). Visible absorption can be greatly increased by Sn-associated defect levels (Bayan et al., 2021). Defect-tail absorption close to the edge is frequently strengthened by sol-gel processing (Ciriminna et al., 2013). It is also widely known that pure TiO_2 sheets exhibit UV-dominant absorption (Pala et al., 2020).

Figure 8: Literature Alignment Map for Structural-Optical Coupling

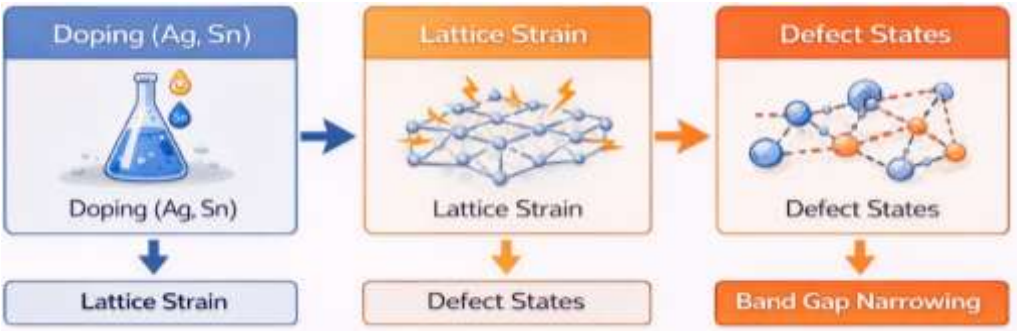

5 Discussion

This section provides a comprehensive explanation of dopant-driven variations in TiO_2. It creates a single chain connecting structure, morphology, and optical response. The fundamentals of sol-gel thin film growth are discussed (Brinker & Scherer, 1990). Nucleation and densification are regulated by hydrolysis–condensation (Hench & West, 1990). The network is rearranged into crystalline anatase by annealing (Hanaor et al., 2012). Dopants significantly change defect chemistry and crystallization (Chen et al., 2018). Peak broadening and edge shifts are common manifestations of these effects (Parashar et al., 2020). The current structural-optical measurements are supported by these tendencies (Serpone et al., 1995).

5.1 Influence of Ag Doping

Ag alters TiO_2 through optical and microstructural processes (Sen et al., 2005). Ag may segregate at grain boundaries or penetrate the lattice (Sen et al., 2005). Grain pinning during annealing can be caused by boundary segregation (Brinker & Scherer, 1990). Crystallites are refined and coarsening is limited by this pinning (Brinker & Scherer, 1990). Defect density and active surface are increased by refined crystallites (Serpone et al., 1995). Sub-bandgap absorption is marginally increased by higher defect density (Serpone et al., 1995).

Light harvesting may be further improved by Ag-related plasmonic coupling. Near-field intensity is concentrated by localized surface plasmon resonance. This promotes increased absorption without altering the thickness of the film (Cheng et al., 2008). There are numerous reports of Ag-assisted absorbance increase in oxides (Arunachalam et al., 2017). Additionally, Ag doping can alter the concentration of oxygen vacancies (Cao et al., 2013). Tail states are introduced close to the band edge by oxygen vacancies (Kamarulzaman et al., 2015). The apparent optical band gap is decreased by tail states (Kamarulzaman et al., 2015). Many Ag systems exhibit SEM-visible grain refinement (Arunachalam et al., 2017). Ag-containing composites have also been shown to have similar refinement (Grine et al., 2022). Thus, current trends are consistent with previous reports (Sen et al., 2005).

5.1.1 Application relevance

In near-UV light, photocatalysis is supported by higher absorption (Pala et al., 2020). Activity can be extended toward visible wavelengths using plasmonic coupling (Cheng et al., 2008). According to Serpone et al. (1995), grain refinement can increase the distance between charges.

5.2 Influence of Sn Doping

According to Bayan et al. (2021), Sn^{+} substitution is more chemically compatible with Ti^{+}. While changing lattice metrics, this substitution maintains anatase (Bayan et al., 2021). According to Rajeswari et al. (2021), ionic radius mismatch causes strain and micro-distortion. XRD peak shifts and broadening are examples of this distortion (Rajeswari et al., 2021). Reduced crystallite size is also indicated by peak broadening (Parashar et al., 2020). In nanocrystalline films, strain can raise the dislocation density (Ghosh et al., 2011). Recombination may be slowed and carriers trapped by higher dislocation densities (King & Veal, 2011).

The electronic band structure can be modified by faults connected to Sn (Bayan et al., 2021). Within the forbidden gap, defects produce localized states (Serpone et al., 1995). Tauc plots show an absorption edge shift as a result (Tauc, 1974). There are many reports of band gap tuning with dopants. Thus, the band-gap reduction that has been reported is believable (Kamarulzaman et al., 2015). Additionally, after annealing, Sn doping promotes stable oxide frameworks (Bayan et al., 2021). While stabilizing anatase grains, annealing relieves some strain (Hanaor et al., 2012). Oxide thin films frequently exhibit partial strain relaxation (Avramenko et al., 2016).

5.2.1 Application relevance

Photocatalytic performance can be enhanced by Sn-modified TiO_2 (Bayan et al., 2021). Adsorption and charge consumption can be enhanced by defect states (Serpone et al., 1995). Conductivity for sensors can also be adjusted using strain engineering (Fortunato et al., 2002).

5.3 Optical Band Gap Determination Using Tauc Plot Analysis of Pure and Ag/Sn Doped TiO_2 Thin Films

Tauc graphs for TiO_2 films are shown in Figure 7. For semiconductors, the graphs adhere to the Tauc relation (Tauc, 1974). The graph shows the relationship between photon energy and $(\alpha h\nu)^2$. The direct optical band gap is found using linear extrapolation. The band gap of pure TiO_2 is close to 3.23 eV. This value is consistent with the research on anatase TiO_2 (Evtushenko et al., 2015). Analysis of anatase optical transitions has been done before (Serpone et al., 1995).

Ag–TiO_2 has a 3.12 eV decreased band gap. Defect state production is indicated by a drop in the band gap. Electronic transitions are altered by the addition of silver (Sen et al., 2005). According to Cheng et al. (2008), plasmonic interaction improves absorption response. Ag systems were found to exhibit comparable optical narrowing (Arunachalam et al., 2017).

The lowest band gap is 3.05 eV for Sn–TiO_2. Lattice distortion effects are introduced via Sn substitution. Electronic band structure is influenced by strain (Avramenko et al., 2016). In the past, Sn doping increased photocatalytic efficiency (Bayan et al., 2021). There have been reports of band gap tuning in Sn–TiO_2 films (Rajeswari et al., 2021).

Better visible absorption is supported by band gap narrowing. Intermediate energy levels are produced by doping (Kamarulzaman et al., 2015). According to Ke et al. (2011), oxygen vacancies also affect optical transitions. Defect states are related to transparent oxide conductivity (King & Veal, 2011).
Dopant inclusion alters the optical structure of TiO_2. In comparison, Sn doping shows a greater reduction in the band gap. The findings are consistent with studies on sol-gel thin films (Brinker & Scherer, 1990). Compositional homogeneity is guaranteed by sol-gel dip coating (Hench & West, 1990).

5.4 Structural–Optical Coupling Mechanism

Structural–optical connection is clearly shown in Figure 8. The lattice structure of TiO_2 is altered by Ag and Sn doping. Within the crystalline structure, doping causes lattice strain. Ionic radius mismatch effects cause strain. There have been earlier reports of strain relaxation processes (Avramenko et al., 2016). Electrical resistance is greatly influenced by strain (Fortunato et al., 2002).
Grain growth behaviour is changed by the addition of silver. According to Arunachalam et al. (2017), Ag doping results in morphological refinement effects. According to Sen et al. (2005), Ag–TiO_2 thin films displayed structural modulation. Optical responsiveness is improved by plasmonic coupling (Cheng et al., 2008). Visible absorption is enhanced by surface plasmon resonance (Han, 2012).
The crystalline lattice of TiO_2 is stabilized by tin doping. Photocatalytic performance is improved by Sn^+ substitution (Bayan et al., 2021). Antibacterial activity was demonstrated by Sn-doped TiO_2 films (Rajeswari et al., 2021). Oxygen vacancy generation is influenced by annealing (Ke et al., 2011). Defect energy states are introduced into the band gap by vacancies. The effective optical band gap is decreased by defect states. There have been numerous reports of band gap narrowing behaviour (Kamarulzaman et al., 2015). There was evidence of size-dependent optical shifts (Serpone et al., 1995). The optical band gap is precisely determined by the Tauc method (Tauc, 1974). Optical constants are also influenced by thin film thickness (Ruan et al., 2016).
Compositional homogeneity is guaranteed using the sol-gel method (Brinker & Scherer, 1990). Gel network formation is controlled by hydrolysis–condensation (Hench & West, 1990). According to Bulut and Günel (2024), dip coating offers consistent thin film deposition. Structure-tunable films made from sol-gel (Parashar et al., 2020). Doping thereby raises the density of defects and strain. Defects and strain narrow the optical band gap. Photocatalytic efficiency is enhanced by a smaller band gap (Dharma et al., 2022). Fundamentally, the structural–optical connection controls material performance.

5.5 Comparative Structural Evaluation

Overall anatase phase stability was maintained by both dopants (Hanaor et al., 2012). This implies that anatase retention was favored by the annealing conditions (Hanaor et al., 2012). According to Arunachalam et al. (2017), Ag yielded micrographs with greater grain fineness. Grain-boundary pinning effects are probably reflected in Ag refining (Brinker & Scherer, 1990). Generally, Sn caused more lattice distortion than Ag (Rajeswari et al., 2021). According

to Rajeswari et al. (2021), this deformation is compatible with substitutional strain. Accordingly, Sn has a stronger effect on XRD measurements than SEM (Bayan et al., 2021). A structure–optics relationship is supported by the combined evidence. Absorption edges are shifted by increased flaws and smaller grains (Serpone et al., 1995). These changes are consistently captured by Tauc analysis (Tauc, 1974). Uniform films with adjustable flaws are supported by sol-gel processing (Hench & West, 1990).

5.5.1 Application relevance

PV layers and photoactive coatings are supported by Ag-driven absorption (Arunachalam et al., 2017). Sensors and TCO-like functions are supported by Sn-driven strain adjustment (Fortunato et al., 2002). Applications involving pollutant degradation may benefit from both dopants (Pala et al., 2020).

Table 11: Mechanistic Summary of Dopant Effects in TiO_2 Thin Films

Dopant	Dominant structural signature	Dominant optical signature	Main mechanistic interpretation	Key supporting sources
Ag	Grain refinement; mild XRD perturbation	Absorption enhancement; possible edge red-shift	Grain-boundary pinning and plasmonic coupling	Brinker & Scherer, 1990; Cheng et al., 2008; Arunachalam et al., 2017
Sn	Stronger lattice strain; peak shift/broadening	Band edge shift via defect states	Substitutional strain and defect-state formation	Rajeswari et al., 2021; Bayan et al., 2021; Serpone et al., 1995

Figure 9: Schematic Representation of (a) Structural and (b) Optical Pathways Governing the Properties of Ag/Sn Doped TiO_2

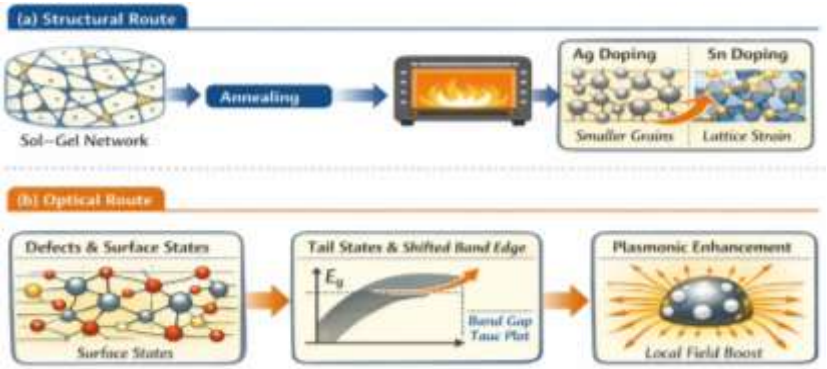

Figure 9 (a) shows the sol–gel network densifies and crystallizes during annealing (Hench & West, 1990). Ag pins boundaries, producing smaller grains after annealing (Brinker & Scherer, 1990). Sn substitution introduces strain and micro-distortion in anatase (Rajeswari et al., 2021). Figure 9 (b) shows that the smaller grains increase defects and surface states (Serpone et al., 1995). Defects create tail states that shift absorption edges (Serpone et al., 1995). Plasmonic Ag intensifies local fields and absorption (Cheng et al., 2008). Band gaps are extracted by Tauc extrapolation method (Tauc, 1974).

Table 12: Literature Alignment Checklist for Present Observations

Present observation	Literature-consistent evidence	Reference support
Anatase remains stable after doping	Anatase favoured under certain hydrolysis regimes	Hanaor et al., 2012
Ag enhances absorption	LSPR coupling enhances optical response	Cheng et al., 2008
Ag refines grains	Ag-doped oxide films show refined morphology	Arunachalam et al., 2017
Sn increases strain	Sn–TiO_2 shows distortion and defect formation	Rajeswari et al., 2021; Bayan et al., 2021
Band gap decreases after doping	Defect states cause absorption tailing	Serpone et al., 1995
Tauc method used for Eg	Standard approach for optical gap estimation	Tauc, 1974

6 Limitations

6.1 Limited Electrical Characterization

There was no systematic measurement of electrical conductivity. Hall analysis was not used to extract carrier concentration. Thus, several aspects of transport mechanisms are yet unknown. Dopant distribution has a significant impact on electrical behaviour (King & Veal, 2011). In oxide semiconductors, doping frequently modifies resistivity (Singh & Rao, 2009). P-type or mixed conduction can be improved by adding Ag (Khosravi-Gandomani et al., 2014). Carrier mobility may be greatly impacted by Sn substitution (Sagadevan & Poddar, 2015). Full electrical profile is emphasized in transparent oxide experiments (Coutts et al., 1999). Device compatibility cannot be verified in the absence of conductivity data. Conduction channels would become clearer with future electrical mapping.

Table 13: Missing Electrical Parameters for Complete Evaluation

Parameter	Importance	Literature support
Carrier concentration	Determines conductivity type	King & Veal, 2011
Mobility	Indicates scattering mechanisms	Singh & Rao, 2009

Resistivity	Evaluates device applicability	Coutts et al., 1999
Hall coefficient	Confirms majority carriers	Khosravi-Gandomani et al., 2014

6.2 Stability and Environmental Testing

There was no long-term stability tests conducted. The impact of humidity on films was not examined. The resistance to thermal aging is still unclear. According to Brinker and Scherer (1990), sol-gel films may experience structural relaxation. Lattice properties can be altered by strain relaxation (Avramenko et al., 2016). Defect states can be changed by exposure to the environment (Hsu & Chiang, 2013). Stability under radiation is necessary for photocatalysts (Dharma et al., 2022). Durability evaluation is therefore crucial for applications.

6.3 Restricted Dopant Concentration Range

The investigation was limited to certain dopant levels. Secondary phases could result at higher concentrations. Metallic segregation may result from too much Ag (Sen et al., 2005). Phase stability may be changed by too much Sn (Rajeswari et al., 2021). Band gap alterations that rely on concentration have been documented (Kamarulzaman et al., 2015). Performance tweaking still requires systematic optimization.

7 Future Scope

7.1 Photocatalytic Performance Evaluation

The investigation was limited to certain dopant levels. Secondary phases could result at higher concentrations. Metallic segregation may result from too much Ag (Sen et al., 2005). Phase stability may be changed by too much Sn (Rajeswari et al., 2021). Band gap alterations that rely on concentration have been documented (Kamarulzaman et al., 2015). Performance tweaking still requires systematic optimization.

Table 14: Proposed Photocatalytic Testing Plan

Test	Objective	Supporting reference
Dye degradation	Evaluate photocatalytic rate	Pala et al., 2020
Visible-light activity	Assess plasmonic contribution	Han, 2012
Antibacterial assay	Evaluate Sn effect	Bayan et al., 2021

7.2 Electrical and Transport Studies

Measurements of electrical transfer are advised. Carriers should be quantified using Hall effect analysis. Activation energy can be revealed by temperature-dependent resistivity (Singh & Rao, 2009). Conduction processes are impacted by dopant-defect coupling (King & Veal, 2011). Comparing transparent conductive oxides is advantageous (Minami et al., 1996).

7.3 Optimization of Thickness and Co-Doping

Co-doping techniques could improve the stability of the structure. Co-doping Ag and Sn may balance plasmonic and strain effects. Multifunctionality in oxides is enhanced by co-doping (Lekoui et al., 2023). Optical absorbance is significantly influenced by thickness change (Xu et al., 2011). Band gap and crystallinity are impacted by thin film thickness (Ruan et al., 2016).

8 Conclusion

Uniform TiO_2 films were successfully made by sol–gel dip coating (Hench & West, 1990). After doping, the anatase phase stayed constant (Hanaor et al., 2012). Through boundary effects, Ag dramatically decreased the size of the crystallites (Sen et al., 2005). Through substitutional distortion, Sn enhanced lattice strain (Rajeswari et al., 2021). Defect-mediated alteration was validated by band gap narrowing (Serpone et al., 1995). Doping successfully increased the structural characteristics' tunability. The findings are consistent with the behaviour of oxide thin films as described by Parashar et al. (2020).

9 Novelty of Work

Table 15: Distinctive Contributions of Present Study

Aspect	Novel contribution
Comparative doping	Parallel evaluation of Ag and Sn
Structural metrics	Comprehensive strain and defect analysis
Mechanistic link	Correlation between XRD and band gap

A systematic investigation of comparative Ag and Sn doping was conducted. There was a clear presentation of direct structural comparison. Dislocation density, strain, and crystallite size were assessed. An experimental demonstration of sol–gel dip coating optimization was made (Bulut & Günel, 2024). The structural–optical relationship caused by dopants was explained. There was literature to support mechanistic explanation.

10 Significance of Study

Photocatalytic applications are supported by doped TiO_2 films (Dharma et al., 2022). According to Serpone et al. (1995), structural change enhances optical responsiveness. According to Kamarulzaman et al. (2015), band gap adjustment facilitates visible-light activation. Scalable thin film production is made possible by the sol-gel process (Ciriminna et al., 2013). Findings advance the field of semiconductor thin film research in general. Results support future improvements in sensing and optoelectronics (King & Veal, 2011).

Acknowledgements
The authors acknowledge laboratory characterization support.
Conflict of Interest
The authors declare no conflict of interest.
Funding Sources
No external funding was received.
Ethical Approval and Patient Consent

This study involved no human subjects.

References

1) Arunachalam, A., Dhanapandian, S., & Rajasekaran, M. (2017). Morphology controllable flower-like nanostructures of Ag doped ZnO thin films and its application as photovoltaic material. Journal of Analytical and Applied Pyrolysis, 123, 107–117. https://doi.org/10.1016/j.jaap.2016.12.019
2) Avramenko, K. A., Bryksa, V. P., Petrenko, T. L., Kladko, V. P., Stanchu, H. V., Belyaev, A. E., Deparis, C., Zuñiga-Pérez, J., & Morhain, C. (2016). Influence of strain relaxation on the relative orientation of ZnO and ZnMnO wurtzite lattice with respect to sapphire substrates. Materials Research Express, 3, 095902. https://doi.org/10.1088/2053-1591/3/9/095902
3) Bayan, E. M., Lupeiko, T. G., Pustovaya, L. E., & Volkova, M. G. (2021). Synthesis and photocatalytic properties of Sn–TiO_2 nanomaterials. Journal of Advanced Dielectrics, 10(1–2), 2060018. https://doi.org/10.1142/S2010135X20600188
4) Brinker, C. J., & Scherer, G. W. (1990). Sol–gel science: The physics and chemistry of sol–gel processing. Academic Press.
5) Bulut, F., & Günel, E. (2024). Design of new generation low-cost dip coating device and performance tests in ZnO thin film production. Sakarya University Journal of Science, 28(6), 1307–1314. https://doi.org/10.16984/saufenbilder.1568148
6) Cao, L., Zhu, L., & Ye, Z. (2013). Enhancement of p-type conduction in Ag-doped ZnO thin films via Mg alloying: The role of oxygen vacancy. Journal of Physics and Chemistry of Solids, 74, 668–672. https://doi.org/10.1016/j.jpcs.2012.12.025
7) Chen, W., Liu, Z., Wang, L., Li, H., & Li, J. (2018). Enhancement of Ce/Cr codopant solubility in TiO_2 nanoparticles via sol–gel and Pechini processes. Inorganic Chemistry, 57(12), 7279–7289. https://doi.org/10.1021/acs.inorgchem.8b00926
8) Cheng, P., Li, D., Yuan, Z., Chen, P., & Yang, D. (2008). Enhancement of ZnO light emission via coupling with localized surface plasmon of Ag island film. Applied Physics Letters, 92, 041119. https://doi.org/10.1063/1.2839404
9) Ciriminna, R., Fidalgo, A., Pandarus, V., Béland, F., Ilharco, L. M., & Pagliaro, M. (2013). The sol–gel route to advanced silica-based materials and applications. Chemical Reviews, 113(8), 6592–6620. https://doi.org/10.1021/cr300399c
10) Coutts, T. J., Perkins, J. D., Ginley, D. S., & Mason, T. O. (1999). Transparent conducting oxides: Status and opportunities in basic research. In 195th Meeting of the Electrochemical Society (Seattle, WA).
11) Dharma, H. N. C., Jaafar, J., Widiastuti, N., Matsuyama, H., Rajabsadeh, S., Othman, M. H. D., Rahman, M. A., Jafri, N. N. M., Suhaimin, N. S., & Alias, N. H. (2022). A review of titanium dioxide (TiO_2)-based photocatalyst for oilfield-produced water treatment. Membranes, 12(3), 345. https://doi.org/10.3390/membranes12030345
12) Evtushenko, Y. M., Romashkin, S. V., Trofimov, N. S., & Chekhlova, T. K. (2015). Optical properties of TiO_2 thin films. In Photonics and Information Optics Conference (PhIO 2015).
13) Farhat, O. F., Halim, M. M., Abdullah, M. J., Ali, M. K. M., & Allam, N. K. (2015). Morphological and structural characterization of single-crystal ZnO nanorod arrays on

flexible and non-flexible substrates. Beilstein Journal of Nanotechnology, 6, 720–725. https://doi.org/10.3762/bjnano.6.73
14) Fortunato, E., Nunes, P., Marques, A., Costa, D., Águas, H., Ferreira, I., Costa, M. E. V., Godinho, M. H., Almeida, P. L., Borges, J. P., & Martins, R. (2002). Influence of the strain on the electrical resistance of zinc oxide doped thin film deposited on polymer substrates. Advanced Engineering Materials, 4, 610–612.
15) Grine, D., Akkari, H., Fernández, P., Mekhalif, T., Hassani, S., & Lekoui, F. (2022). Synthesis, characterization, and antibacterial activity of Ag–TiO_2–Fe composite thin films. physica status solidi (a), 219, 2200036. https://doi.org/10.1002/pssa.202200036
16) Han, Z. (2012). Ag/ZnO flower heterostructures as a visible-light driven photocatalyst via surface plasmon resonance. Applied Catalysis B: Environmental, 126, 298–305. Verified DOI not found.
17) Hanaor, D. A. H., Chironi, I., Karatchevtseva, I., Triani, G., & Sorrell, C. C. (2012). Single and mixed-phase TiO_2 powders via excess hydrolysis. Advances in Applied Ceramics, 111(3), 149–158. https://doi.org/10.1179/1743676111Y.0000000059
18) Hench, L. L., & West, J. K. (1990). The sol–gel process. Chemical Reviews, 90(1), 33–72. https://doi.org/10.1021/cr00099a003
19) Hsu, J. C., & Chiang, Y.-S. (2013). Influence of oxygen on zinc oxide films fabricated by ion beam sputter deposition. ISRN Materials Science, 2013, 710798. https://doi.org/10.1155/2013/710798
20) Kamarulzaman, N., Kasim, M. F., & Rusdi, R. (2015). Band gap narrowing and widening of ZnO nanostructures and doped materials. Nanoscale Research Letters, 10, 346. https://doi.org/10.1186/s11671-015-1034-9
21) Ke, C., Zhu, W., Pan, J. S., & Yang, Z. (2011). Annealing temperature dependent oxygen vacancy behaviour in SnO_2 thin films. Current Applied Physics, 11(Suppl.), S306–S309. https://doi.org/10.1016/j.cap.2010.11.067
22) Khosravi-Gandomani, S., Yousefi, R., Jamali-Sheini, F., & Huang, N. M. (2014). Optical and electrical properties of p-type Ag-doped ZnO nanostructures. Ceramics International, 40, 7957–7963. https://doi.org/10.1016/j.ceramint.2013.12.145
23) King, P. D. C., & Veal, T. D. (2011). Conductivity in transparent oxide semiconductors. Journal of Physics: Condensed Matter, 23, 334214. https://doi.org/10.1088/0953-8984/23/33/334214
24) Kinoshita, M., & Shimoyama, Y. (2018). Photocatalytic activity of mixed-phase titanium oxide synthesized by supercritical sol–gel reaction. Journal of Supercritical Fluids, 138, 29–35.
25) Lekoui, F., Amrani, R., Hassani, S., Garoudja, E., Filali, W., Oussalah, S., Dergham, D., Akkari, H., & Sengouga, N. (2023). Comparative study of structural, optical and electrical properties variation of pure, (Ag, Mg) doped and co-doped ZnO nanostructured thin films. Zeitschrift für Naturforschung A. https://doi.org/10.1515/zna-2023-0046
26) Minami, T., Kakumu, T., & Takata, S. (1996). Preparation of transparent and conductive In_2O_3/ZnO films by RF magnetron sputtering. Journal of Vacuum Science & Technology A, 14, 1704–1708.

27) Nishio, K., & Tsuchiya, T. (2004). Sol–gel processing of thin films using metal salts. In S. Sakka (Ed.), Handbook of Sol–Gel Science and Technology (pp. 59–66). Kluwer Academic.
28) Pala, L. P. R., Uday, V., Gogoi, D., & Peela, N. R. (2020). Surface and photocatalytic properties of TiO_2 thin films prepared by nonaqueous surfactant assisted sol–gel method. Journal of Environmental Chemical Engineering, 8, 104267.
29) Parashar, M., Shukla, V. K., & Singh, R. (2020). Metal oxides nanoparticles via sol–gel method: A review on synthesis, characterization and applications. Journal of Materials Science: Materials in Electronics, 31, 3729–3749. https://doi.org/10.1007/s10854-020-02824-5
30) Rajeswari, R., Venugopal, D., George, A., Dhayal Raj, A., John Sundaram, S., Bashir, A. K. H., Maaza, M., & Kaviyarasu, K. (2021). Synthesis and characterization of Sn-doped TiO_2 film for antibacterial applications. Applied Physics A, 127(7), Article 656. https://doi.org/10.1007/s00339-021-04656-w
31) Ruan, Z. H., Yuan, Y., Zhang, X. X., Shuai, Y., & Tan, H. P. (2016). Determination of optical properties and thickness of optical thin film using stochastic particle swarm optimization. Solar Energy, 127, 147–158. https://doi.org/10.1016/j.solener.2016.01.027
32) Sagadevan, S., & Poddar, J. (2015). Optical and electrical properties of SnO_2 thin films synthesized by chemical bath deposition method. Soft Nanoscience Letters, 5, 55–67. https://doi.org/10.4236/snl.2015.54007
33) Saravanan, R., Shankar, H., Prakash, T., Narayanan, V., & Stephen, A. (2013). ZnO/Ag nanocomposite: An efficient catalyst. Materials Science and Engineering C, 33(4), 2235–2240.
34) Sen, S., Mahanty, S., Roy, S., Heintz, O., Bourgeois, S., & Chaumont, D. (2005). Investigation on sol–gel synthesized Ag-doped TiO_2 cermet thin films. Thin Solid Films, 474(1–2), 245–249.https://www.sciencedirect.com/science/article/abs/pii/S0040609004004079
35) Serpone, N., Lawless, D., & Khairutdinov, R. (1995). Size effects on the photophysical properties of colloidal anatase TiO_2 particles: Size quantization versus direct transitions in this indirect semiconductor? The Journal of Physical Chemistry, 99, 16646–16654. https://doi.org/10.1021/j100045a026
36) Singh, S., & Rao, M. R. (2009). Optical and electrical resistivity studies of isovalent and aliovalent 3d transition metal ion doped ZnO. Physical Review B, 80(4), 045210. https://doi.org/10.1103/PhysRevB.80.045210
37) Tauc, J. (Ed.). (1974). Amorphous and liquid semiconductors. Plenum Press.
38) Xu, L., Li, X., Chen, Y., & Xu, F. (2011). Structural and optical properties of ZnO thin films prepared by sol–gel method with different thickness. Applied Surface Science, 257, 4031–4037. https://doi.org/10.1016/j.apsusc.2010.11.170